# Fabrication and Characterisation of a Large-Area Solid Oxide Fuel Cell Based on Dual Tape Cast YSZ Electrode Skeleton Supported YSZ Electrolyte with Vanadate and Ferrite Perovskite-Impregnated Anode and Cathode

By C.S. Ni[a], J.M. Vohs[b], R. J. Gorte[b] and J. T.S. Irvine[a]*

[a]School of Chemistry, University of St Andrews, Fife KY16 9ST, Scotland.

*Corresponding author: E-mail: jtsi@st-andrews.ac.uk

[b]Department of Chemical Engineering, University of Pennsylvania, Philadelphia, PA 19104 (USA)

## Abstract

Infiltration of ceramic materials into a pre-formed ceramic scaffold is an effective way of fabricating a solid oxide fuel cell with nano-structured ceramic electrodes by avoiding detrimental interfacial reactions through low-temperature processing for achieving high performance using hydrogen as well as carbonaceous fuel. However, there are, however, significant concerns about the applicability of this method because of the difficulty in fabricating a large-area gas-tight but thin electrolyte between two highly porous ceramic and the multiple repetitions of infiltration process. Here, a large-area (5 cm by 5 cm) scaffold with a thin yttria-stabilized zirconia (YSZ) electrolyte sandwiched between two identical porous structures is prepared by tape casting and co-firing, and then solution precursors are impregnated into the porous scaffolds to prepare nano-structured $La_{0.8}Sr_{0.2}FeO_3$ (LSF) and $La_{0.7}Sr_{0.3}VO_{3-\delta}$ (LSV$_{red}$). The thus prepared solid oxide fuel cell with 10 wt.% ceria + 1 wt.% Pd as catalyst in anode shows a peak power of 489 mW/cm$^2$ (~6 W per cell) at 800 $^o$C using H$_2$ as fuel and air as oxidant. This large-area fuel cell retained the integrity of the thin electrolyte and high performance after the reducing-oxidation cycle at 900 $^o$C, showing superiority over the conventional Ni(O)-YSZ based support.

Keywords: solid oxide fuel cell, infiltration, ceramic electrode, YSZ

## Introduction

Fuel cells are the most efficient electrochemical device to directly convert stored chemical energy to usable electrical energy [1,2]. Compared to proton membrane exchange fuel cells (PEMFCs) that require pure hydrogen as fuel, solid oxide fuel cells (SOFCs), utilizing an oxygen ion conducting electrolyte, can oxidize either hydrogen or hydrocarbon fuels. In the last decade, much effort has been devoted to developing

conductive oxide-based anodes (e.g. (La, Sr) TiO$_3$ [3,4], (La, Sr) (Cr, Mn) O$_{3-\delta}$ [5,6] and Sr$_2$Mg$_{1-x}$Mn$_x$MoO$_{6-\delta}$ (x=0-1) [7]) to enhance the fuel flexibility of SOFCs because they are more stable against carbon formation in hydrocarbon-based fuels and less sensitive to oxidation and reduction (redox) cycles than the state-of-the-art Ni (O) cermet does. However, two major problems are associated with the ceramic anode. First, compared with Ni (O) cermet, the electrode-performance characteristics of most of these materials are poor at intermediate temperatures (600-800 $^o$C) because many of these oxides are not good catalysts for the oxidation of the fuel [8]. The introduction of reducible transition metals into the functional layer is one approach that can be used to enhance the catalytic activity [9]. The infiltration of ceramic conductors and catalytic metals (e.g. Ni, Pt and Pd) into porous scaffolds that had been pre-sintered onto the electrolyte is regarded as an effective method of promoting the electrode performance via producing nano-scale particles by in-situ sintering at relatively low temperatures [10,11, 12,13]. The nano-scale particles are able to increase the length of triple phase boundaries (TPBs) that provide the reaction sites for the fuel oxidation [14]. Second, the low conductivity of most ceramics in a fuel environment prohibits a configuration with a thick anode because of the large ohmic losses that it might cause [14]. In this study, we decided to use La$_{0.7}$Sr$_{0.3}$VO$_{3-\delta}$ (LSV$_{red}$) as the anode material as it has recently been shown to provide good electronic conductivity in scaffold configuration [15,16,17]. For example, the effective electronic conductivity of 30 wt. % LSV$_{red}$ impregnated into an YSZ scaffold was reported to be higher than 1 S cm$^{-1}$ for porous bodies at 700 $^o$C [16].

The breakthrough of utilization of infiltration as a practical method in producing nano-structured ceramic electrode lies in the scaling up for mass production of commercial devices, as lots of effort has been devoted to developing infiltration as an effective way of fabricating high-performance electrodes and avoiding the undesired solid-state reaction between the perovskite and YSZ as in conventional sintering process of composite electrodes [18]. Scaling up this new design from its tablet-size prototype to a full-size fuel cell would be a large step toward making a SOFC of high performance and more fuel flexible. Unfortunately, the scaling up of infiltration is difficult because of the intrinsic idiosyncrasies of this method. First, the fabrication of a thin watertight electrolyte of large area on a highly porous substrate is, in fact, a primary challenge in the co-sintering of powders via cost-effective method [19]. The highly porous support is frailer than a Ni(O)-YSZ support and no weight can be put onto it to make it flat. Second, the infiltration process usually requires multiple infiltrations and pre-sintering steps [20] to deposit enough oxides to form a conductive layer of interconnected particles, and it is unknown if the porous scaffold on a large-scale cell will survive the repetitions of thermal cycling or if the solution will be evenly distributed over the large-area porous structure. Finally, the transport of solution in several hundred micrometers of pore structure to the electrode/electrolyte interface is another concern in the mass production of large-scale anode- or cathode-supported SOFCs [21].In this study, however, we demonstrate that scalable and cost-effective tape casting can be used to prepare the flat large-area dense electrolyte on porous scaffold and then concentrated aqueous

solutions of precursors can be used to impregnate the cathode and anode before each pre-sintering to obtain a loading of 25 wt. % $La_{0.7}Sr_{0.3}VO_{4-\delta}$ ($LSV_{ox}$) for anode and 35 wt.% $La_{0.8}Sr_{0.2}FeO_3$ (LSF) for cathode in ten impregnations. In order to avoid infiltrating one very thick support, we choose to impregnate two identical YSZ scaffolds for cathode and anode.

**Experimental section**

Slurry for the green tapes of electrolyte was prepared by milling the YSZ (HSY-8, DKKK, Japan) with binder (Polyvinyl butyral) and plasticizers (Polyethylene glycol and Di-n-butyl phthalate) in ethanol – Methyl Ethyl Ketone solvent and then cast on to a Mylar paper. Two layers of green tape containing YSZ and 65 wt % and 85 wt. % graphite (compared to the weight of YSZ) were cast sequentially on the top of the ysz green tape with 1-hour interval for drying [22].Two co-cast green tapes were laminated together (Figure 1 (a)) to produce a tri-layer green tape for YSZ wafer. The green tapes were fired at 1400 $^o$C for 5 hours on a zirconia plate to prepare the scaffold for impregnation (Figure 1 (b)). In order to avoid the warping of the large-area scaffold, the green tape is in between two zirconia plates. A group of thin wedges or spacers is placed beside the green tape to avoid the direct crush of zirconia plate on the porous structure and zirconia tape and to allow scalability in a stack system, as shown in Figure S1. In our lab four scaffolds can be produced in each batch.

Stoichiometric amounts of $La(NO_3)_3.6H_2O$, $Sr(NO_3)_2$, $NH_4VO_3$ and $Fe(NO_3)_3.9H_2O$ were dissolved in de-ionized water together with citric acid (1:1 mole to metallic ion) for the impregnation of $La_{0.8}Sr_{0.2}FeO_3$ (LSF) and $La_{0.7}Sr_{0.3}VO_{4-\delta}$ ($LSV_{ox}$). Considering the low solubility of metavanadate in water at room temperature, the solution for $LSV_{ox}$ was heated up to 60 $^o$C on a hot plate and then impregnated into one side of the porous scaffold, followed by the impregnation of LSF on the other side of the scaffold. The scaffold with the content is pre-sintered hereafter at 700 $^o$C for 30 minutes after each impregnation. Ten impregnations had been performed to get the loading of LSF and $LSV_{ox}$ reaching 35 wt. % and 25 wt. %, respectively. For the cell with catalyst, solution of Ce nitrate and Pd nitrate were impregnated into the anode after the final 700-$^o$C firing, followed by a firing at 500 $^o$C. Pt paste ((Gwent, C2000904P3)) was applied on both sides of the electrode and then the whole cell was fired at 900 $^o$C for 30 min to densify the Pt paste and produce the correct phase of the perovskite.

A single cell was tested on a non-sealing device (ECN type) that uses $N_2$ around the edges of cathode side of the cell as a separating gas [23]. The arrangement of the testing satiation is shown in Figure S2. A weight of 4 kg was put onto the cell to improve contact after the installation. Because the fuel cell will be sandwiched in between two flat alumina bodies, the fuel cell has to be flat enough to avoid being cracked by the pressure.The sample was heated up to 700 $^o$C at a ramp rate of 1 $^o$C min$^{-1}$, and then wet hydrogen (4.3 % $H_2O$) was applied to replace the initial nitrogen flow on the anode to allow a 2-hour reduction. The flow rate

of air was 2500 ml min$^{-1}$ and those of pure oxygen and hydrogen were 500 ml min$^{-1}$. For the thermal and redox cycle, the tested fuel cell was taken out of the testing device, fired at 900 $^{o}$C for 30 min and tested again. Electrochemical characterization was performed under ambient pressure. Ac impedance measurement was carried out on a Solartron 1260 frequency response analyzer (FRA) by applying a sine signal of 10 mV in the range from 10 kHz to 0.04 Hz. The IV curve was retrieved by a Kikusui Electronic Load. The reflective XRD pattern was recorded on a PANalytical X-ray diffractometer with graphite-monochromatized Cu Kα radiation (λ = 1.5418 Å), employing a scan rate of 1.5 deg. min$^{-1}$ in the 2$\theta$ range of 10° to 100°. The diffraction data were refined by the Rietveld method, using the program General Structure Analysis System (GSAS). The microstructure and composition of the electrodes was inspected by SEM on a JEOL 6700F scanning electron microscope with an Energy-dispersive X-ray spectroscopy (EDS). Some of the samples were mounted in an epoxy and then polished for backscattering electron imaging. The measurement of porosity was carried out on the back-scattering images with the software ImageJ (National Institute of Health, Bethesda, MD).
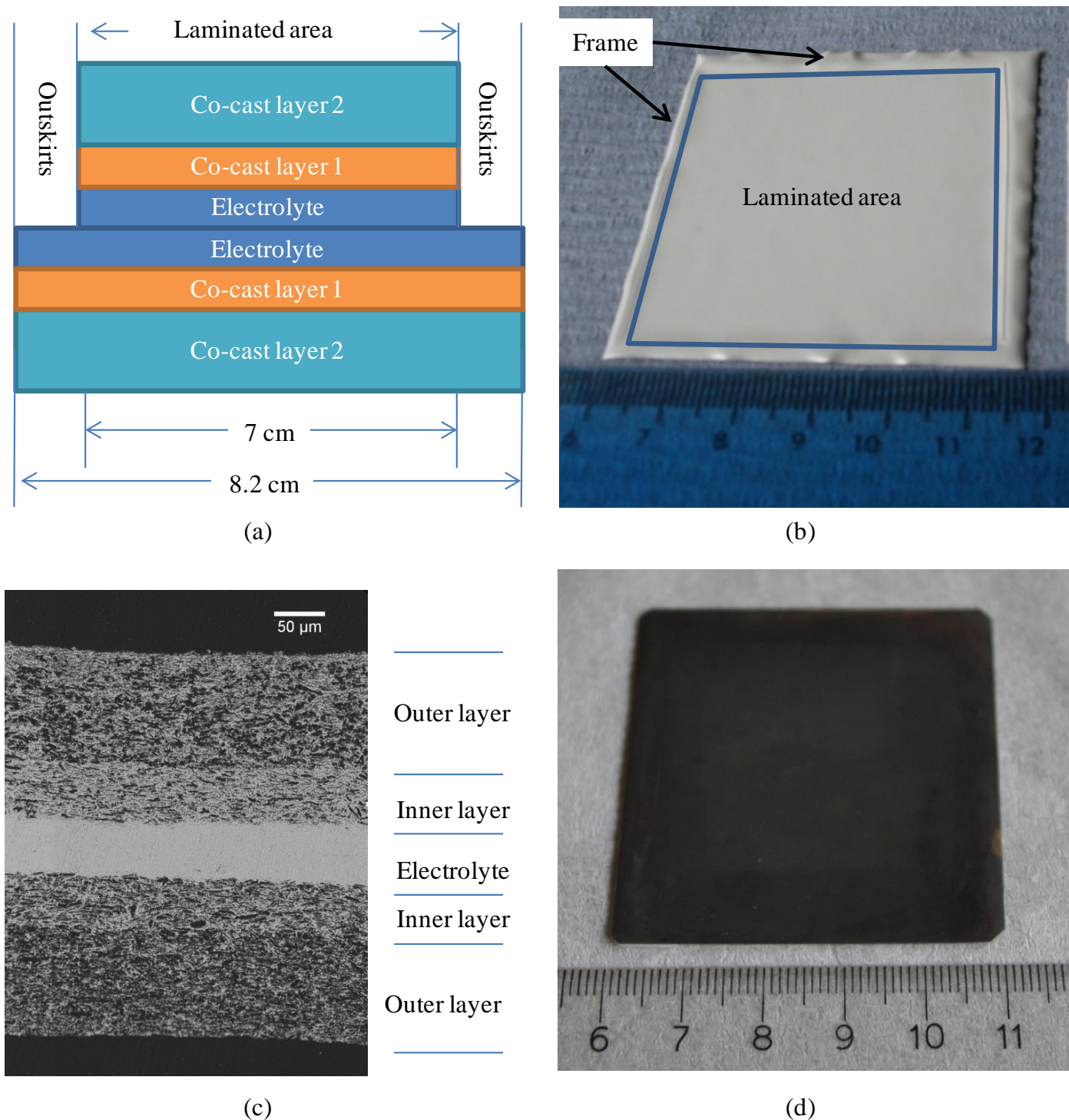
## Result and discussion



Figure 1. (a) Schematic illustration of the lamination of the YSZ green tapes with two co-cast layers containing YSZ and varied amount of graphite; (b) the scaffold sintered at 1400 $^o$C having a flat laminated area and a warping frame from the outskirts of green tapes; (c) SEM cross-section of the scaffold with a dense electrolyte and two identical gradient porous structure for the electrodes; (d) image of the fuel cell (cathode side) after impregnation and scraping off the frame.

The scheme (Figure 1 (a)) illustrates the lamination of the co-cast green tapes for co-sintering. Since YSZ powder from the same batch is the only ceramic involved in the sintering process at elevated temperature,

the mismatch in the rate of shrinkage is less a concern than that in the co-sintering of different materials. The outer edge of the sintered scaffold (Figure 1 (b)) contains a stretching frame from the outskirt of the larger green tape that enables the large central flat laminated area, with only the outer edge being constrained during sintering. A sample without the outer edge is shown in Figure S3, which indicates that the whole sample is deformed, showing radial gutters originating from the center of the porous scaffold. The microstructure (Figure 1 (c)) of the scaffold contains a 55-μm electrolyte sandwiched between two identical YSZ layers of gradient porosity; the porous inner layer in contact with electrolyte is 52 % porous (48-μm thick) measured by image analysis and the outer layer is 67 % porous (112-μm thick). This graded design is beneficial for producing a dense electrolyte on the porous structure while providing enough porosity for mass transport [21,24]. The low porosity of the inner layer with smaller pores can also increase the surface area for the impregnated particles to sit on and decrease the pore size for smaller interface resistance. After impregnation, the frame was rubbed off to produce a 5 cm by 5 cm fuel cell (Figure 1 (d)).

The XRD patterns of the strontium-doped lanthanum vanadate (LSV)-YSZ electrode before and after reduction are shown in Figure S4, confirming the conversion of $LSV_{ox}$ into $LSV_{red}$ after reduction in the fuel at 800 $^o$C. The reduction of monazite $LSV_{ox}$ is reported to occurred readily at an oxygen fugacity, $10^{-18}$ atm., below 700 $^o$C [25] to produce an electrically conductive perovskite $LSV_{red}$. The The cell parameters of the $LSV_{red}$ in YSZ porous structure are calculated by refining the high-intensity XRD data of $LSV_{red}$/YSZ, as shown in Figure S5. The structure of infiltrated $LSV_{red}$ is refined as orthorhombic with a=5.5326(4) Å, b=7.8237(5) Å, c=5.5499(2) Å and $V$= 240.23 Å. The volume of the unit cell of $La_{0.7}Sr_{0.3}VO_{3-\delta}$ is slightly larger than that reported for $La_{0.9}Sr_{0.1}VO_{3-\delta}$[26], 240.16 Å$^3$. The incorporation of a $Sr^{2+}$ at the position of $La^{3+}$ should expand the unit cell due to the larger ion radius of $Sr^{2+}$. Even though pure $La_{0.7}Sr_{0.3}VO_3$ crystals are observed with calcination at 2000 $^o$C under $Ar/H_2$ gas[27], the annealing of $La_{0.7}Sr_{0.3}VO_{4-\delta}$ will eventually lead to phase separation and the appearance of $SrVO_3$ in addition to the orthorhombic $LaVO_3$ phase in the temperature range of 800-1100 $^o$C[26,28] under reduction with $H_2$. The refinement in this study is not able to eliminate the existence of traces of cubic $Sr_{1-x}La_xVO_3$ (x<0.5) or tetragonal $Sr_3V_2O_7$ phase.
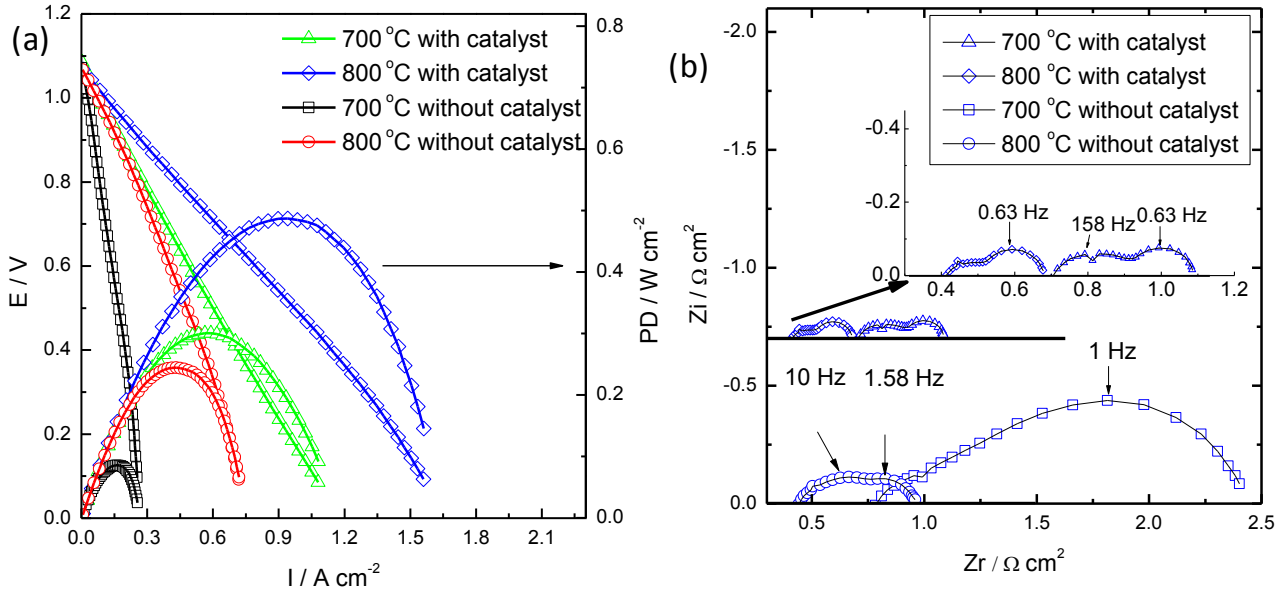
Figure 2. Performance of an ceramic impregnated large fuel cell with and without ceria + Pd as catalyst under wet (4.2 vol. % $H_2O$) $H_2$ fuel. (a) I – V and I – P curves; (b) Nyquist plots of impedance spectra. The gas flow rates were 2.5 L/min air and 500 ml/min wet $H_2$. The insert in (b) is the magnified plot for the cell with ceria + Pd as catalyst.

Impregnated cells with a current-collected area of 3.5 cm x 3.5 cm were electrochemically characterized at 700-800 $^{o}$C using humidified $H_2$ (4.2 vol. % $H_2O$) as fuel and air as oxidant. In Figure 2 (a), the open circuit voltages (OCVs) are above 1.07 V at both temperatures for all cells with or without impregnation of 10 wt.% ceria + 1 wt.% Pd as catalyst. Considering the non-sealing property of the ECN-type testing station (see experimental section), this OCV is high enough to imply a dense electrolyte. The maximum power densities (Figure 2 (a)) for the cell without catalysts on the anode side are 84 mW cm$^{-2}$ and 245 mW cm$^{-2}$ at 700 $^{o}$C and 800 $^{o}$C, respectively. The addition of 10 wt.% ceria + 1 wt.% Pd enhances the performance significantly: high power densities of 300 mW cm$^{-2}$ and 489 mW cm$^{-2}$ are achieved at 700 $^{o}$C and 800 $^{o}$C, respectively. The maximum power is 6 W for a single cell at 800 $^{o}$C. Of the limited demonstrations on large-area fuel cells prepared by infiltration technique, the performance of this fuel cell at 700 $^{o}$C is comparable to the one with a sintered Ni(O)-YSZ support and an $La_{0.6}Sr_{0.4}Co_{0.2}Fe_{0.8}O_3$-infiltrated YSZ cathode that shows a peak powder density of 350 mW cm$^{-2}$ [29]. However, this is the first demonstration of large area fuel cells with ceramic anode and with infiltration for both cathode and anode. Comparing with the cell without catalyst, the dramatic decrease of the electrode polarization resistance, $R_p$, which is represented by the distance between the high and low frequency intercepts of the curve with the real impedance axis (Fig. 2 (b)), confirms that the high electrode losses come from the anode of the cell without catalyst. In order to study the contribution of the cathode losses, pure oxygen is used as the oxidant for the cell with 10 wt.% ceria + 1 wt.% Pd in the anode. The slope of the IV curve (Figure 3 (a)) and the $R_p$ estimated from

impedance plot (Figure 3(c)) change slightly with the increase of the partial pressure of oxygen, indicating that 160-μm cathode contributes only an small part to the $R_p$ in the region above 0.7 V.
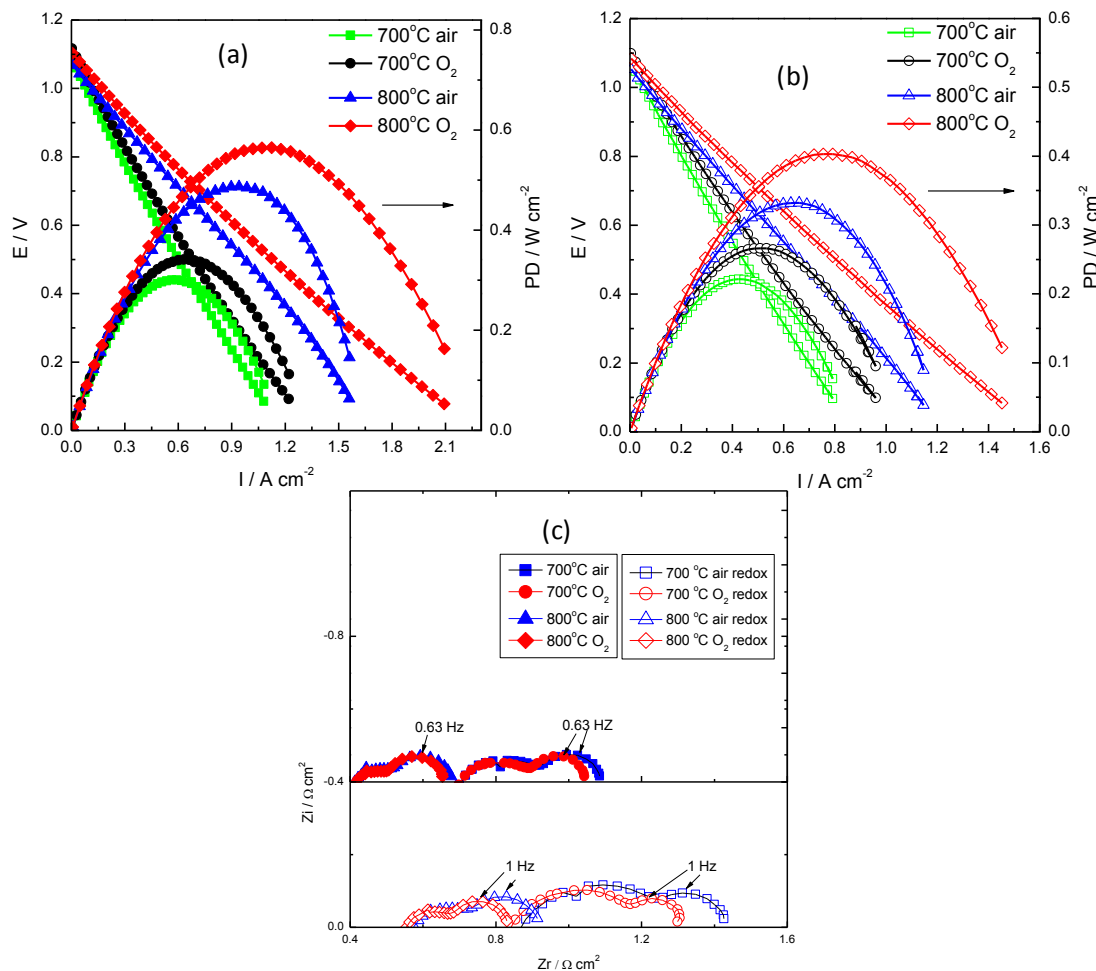


Figure 3. Performance of fuel cell with ceria + Pd as catalyst under air or oxygen as oxidant before (a) and after (b) redox cycle at 900 °C. (c) Nyquist plots of impedance spectra at OCV under air or oxygen as oxidant.

The performance of the fuel cell after thermal and redox cycle at 900 °C is shown in Figure 3(b). The maximum power density at 700 °C decreases to 220 mW cm$^{-2}$, but the OCV does not change, meaning the conversion between LSV$_{red}$ and LSV$_{ox}$ does not exert any damage to the integrity of the electrolyte, in contrast to the electrolyte on the nickel cermet-supported fuel cell [30].The sintering of nano particles, especially metallic Pd, might be a concern at a redox temperature as high as 900 °C[31], but the ceramic-impregnated fuel cell can still be used at intermediate temperatures. The redox cycle is supposed to change the microstructure of the anode, including LSV$_{red}$, ceria and Pd [32], but the sintering of LSF on the cathode

side can also contribute to the increase of impedance because the difference of the partial pressure of oxygen exerts greater influence on the $R_p$ value, as shown in Figure 3 (c).
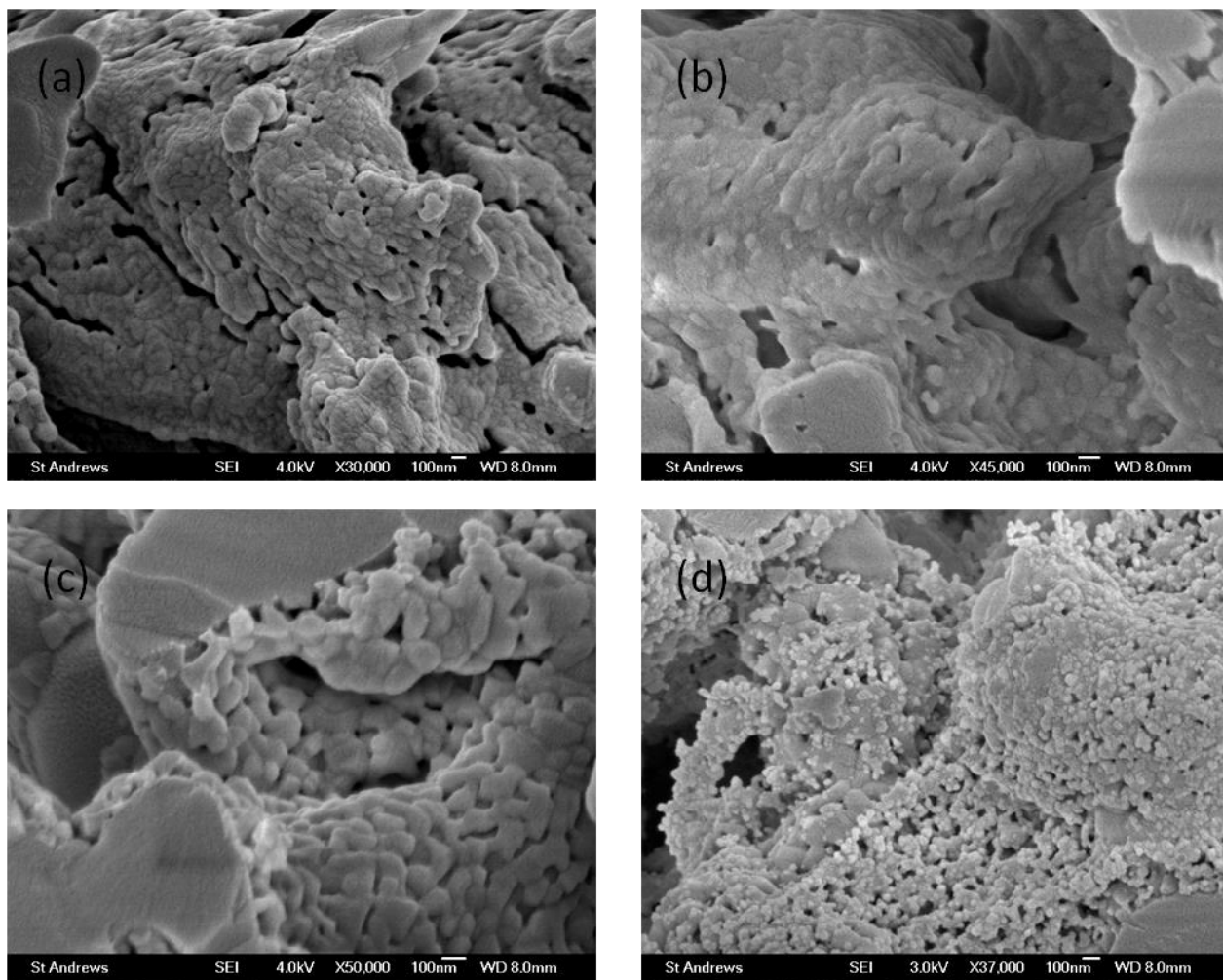


Figure 4. SEM images of LSF/ YSZ (a), LSV$_{ox}$/YSZ (b) and post-test LSV$_{red}$/YSZ (c) electrode; (d) is that of LSV$_{ox}$ / YSZ with ceria and Pd after a calcination at 900 $^o$C for 30 min. The white particles in (d) are Pd nano particles.

Figure 4 shows the SEM images of the electrodes. After the calcination at 900 $^o$C in air, both the LSV$_{ox}$ and LSF form a coating of 100 nm particles on the surface of YSZ. Similar to the observation of LSCM on YSZ[33] after firing in air and then reduction, LSV$_{red}$ particles contracted in humidified H$_2$ at 800 $^o$C, exposing the underneath YSZ scaffold partially to the fuel. This phenomenon demonstrates an increase of active surface occurring under operational conditions. This morphology can decrease the electronic conductivity of the LSV$_{red}$ structure but provide more TPBs for electrochemical reaction. The ceria particles supporting the Pd particles of approximately 20 nm form a porous network on the surface of LSV$_{ox}$ after calcinations at 900 $^o$C which is thought to inhibit the poisoning of metal catalyst caused by direct contact with vanadium and slow down the growth of Pd nanoparticles [15,31].

## Conclusion

In conclusion, a 5 cm by 5cm flat tri-layer scaffold of YSZ has been prepared using the inexpensive and scalable tape casting method and impregnated with perovskites for cathode and anode. The configuration of gradient porosity and identical scaffold for cathode and anode simplifies the sintering process and the impregnation process. Furthermore, the fuel cell shows excellent performance thanks to the nano-sized perovskite formed at intermediate temperatures and the 160-μm cathode does provide sufficient mass transport of oxygen and does not limit the performance of the cell.

## Acknowledgement

# References

[ 1 ] Fuel cell handbook 7th edition. . U.S. Department of Energy; 2004. http://www.netl.doe.gov/technologies/coalpower/fuelcells/seca/pubs/FCHandbook7.pdf.

[2] N. Q. Minh, *J. Am. Ceram. Soc.*, 1993, **76**, 563-588.

[3] O. A. Marina, N. L. Canfield and J. W. Stevenson, *Solid State Ionics*, 2002, **149**, 21-28.

[4] J. C. Ruiz-Morales, J. Canales-Vázquez, C. Savaniu, D. Marrero-López, W. Zhou and J. T. S. Irvine, *Nature*, 2006, **439**, 568-571.

[5] S. Tao and J. T. S. Irvine, *Nat. Mater.*, 2003, **2**, 320-323.

[6] S. W. Tao, J. T. S. Irvine and J. A. Kilner, *Adv. Mater.*, 2005, **17**, 1734-1737.

[7] Y. H. Huang, R. I. Dass, Z. L. Xing and J. B. Goodenough, *Science*, 2006, **312**, 254-257.

[8] R. J. Gorte, J. M. Vohs, *Annu. Rev. Chem. Biomol. Eng.*, 2011, **2**, 9-30.

[9] G. Kim, S. Lee, J. Y. Shin, G. Corre, J. T. S. Irvine, J. M. Vohs, R. J. Gorte, *Electrochem. Solid State Lett.*, 2009, **12**, B48- B52.

[10] R. J. Gorte, S. Park, J. M. Vohs, C. Wang, *Adv. Mater.*, 2000, **12**, 1465- 1469.

[11] T. Z. Sholklapper, H. Kurokawa, C. P. Jacobson, S. J. Visco and L. C. De Jonghe, *Nano Lett.*, 2007, **7**, 2136-2141.

[12] S. P. Jiang, *Int. J. Hydrogen Energy*, 2012, **37**, 449-470.

[13] R. J. Gorte and J. M. Vohs, *Curr. Opin. Colloid Interface Sci.*, 2009, **14**, 236-244.

[14] A. Atkinson, S. Barnett, R. J. Gorte, J. T. S. Irvine, A. J. McEvoy, M. Mogensen, S. C. Singhal and J. Vohs, *Nat. Mater.*, 2004, **3**, 17-27.

[15] J.-S. Park, I. D. Hasson, M. D. Gross, C. Chen, J. M. Vohs and R. J. Gorte, *J. Power Sources*, 2011, **196**, 7488-7494.

[16] Z. Cheng, S. Zha, L. Aguilar and M. Liu, *Solid State Ionics*, 2005, **176**, 1921-1928.

[17] L. Adijanto, V. Balaji Padmanabhan, K. J. Holmes, R. J. Gorte and J. M. Vohs, *J. Solid State Chem.*, 2012, **190**, 12-17.

[18] J. M. Vohs and R. J. Gorte, *Adv. Mater.,* 2009, **21**, 943-956.

[19] L. C. De Jonghe, C. P. Jacobson and S. J. Visco, *Annu. Rev. Mater. Res.*, 2003, **33**, 169-182.

[20] T. Z. Sholklapper, C. P. Jacobson, S. J. Visco and L. C. De Jonghe, *Fuel Cells*, 2008, **8**, 303-312.

[21] L. K. Taek, H. S. Yoon, J. S. Ahn and E. D. Wachsman, *J. Mater. Chem.*, 2012, **22**, 17113-17120.

[22] S. Le, K. N. Sun, N. Zhang, X. Zhu, H. Sun, Y. X. Yuan and X. Zhou, *J. Power Sources*, 2010, **195**, 2644-2648.

[23] M. C. Verbraeken, B. Iwanschitz, A. Mai and J. T. S. Irvine, *J. Electrochem. Soc.*, 2012, **159**, F757-F762.

[24] C. M. An, J.-H. Song, I. Kang and N. Sammes, *J. Power Sources*, 2010, **195**, 821-824.

[25] P. R. Shah, M. M. Khader, J. M. Vohs and R. J. Gorte, *J. Phys. Chem. C*, 2008, **112**, 2613-2617.

[26] X. M. Ge and S. H. Chan, *J. Electrochem. Soc.,*2009, **156,** B386-B91.

[27] M. Sayer, P. Chen, R. Fletcher, and A. Mansingh, *J of Phys.C: Solid State Phys.,* 1975, **8,** 2059-2071.

[28] M. Kestigian, J. G. Dickinson, and R. Ward, *J. Am. Chem. Soc.,*1957, **79**, 5598-601.

[29] J. Chen, F. Liang, D. Yan, J. Pu, B. Chi, S. P. Jiang and L. Jian, *J. Power Sources*, 2010, **195**, 5201-5205.

[30] M. Cassidy, G. Lindsay and K. Kendall, *J. Power Sources*, 1996, **61**, 189-192.

[31] J. S. Kim, N. L. Wieder, A. J. Abraham, M. Cargnello, P. Fornasiero, R. J. Gorte and J. M. Vohs, *J. Electrochem. Soc.*, 2011, **158**, B596-B600.

[32] J.-S. Park, J. Luo, L. Adijanto, J. M. Vohs and R. J. Gorte, *J. Power Sources*, 2013, **222**, 123-128.

[33] G. Corre, G. Kim, M. Cassidy, J. M. Vohs, R. J. Gorte and J. T. S. Irvine, *Chem. Mater.*, 2009, **21**, 1077-1084.

**Captions of figures**

Figure 1. (a) schematic illustration of the lamination of the YSZ green tapes with two co-cast layers containing YSZ and varied amount of graphite; (b) the scaffold sintered at 1400 $^{o}$C having a flat laminated area and a warping frame from the outskirts of green tapes; (c) SEM cross-section of the scaffold with a dense electrolyte and two identical gradient porous structure for the electrodes; (d) image of the fuel cell (cathode side) after impregnation and scraping off the frame.

Figure 2. Performance of an impregnated large fuel cell with and without ceria + Pd as catalyst under wet (4.2 vol. % $H_2O$) $H_2$ fuel. (a) I – V and I – P curves; (b) Nyquist plot of impedance spectra. The gas flow rates are 2.5 L/min air and 500 ml/min wet $H_2$. The insert in (b) is the magnified plot for the cell with ceria + Pd as catalyst.

Figure 3. Performance of fuel cell with ceria + Pd as catalyst under air or oxygen as oxidant before (a) and after (b) redox cycle at 900 $^{o}$C. (c) Nyquist plots of impedance spectra under air or oxygen as oxidant.

Figure 4. SEM images of LSF/ YSZ (a), $LSV_{ox}$/YSZ (b) and post-test $LSV_{red}$/YSZ (c) electrode; (d) is that of $LSV_{ox}$ / YSZ with ceria and Pd after a calcination at 900 $^{o}$C for 30 min. The white particles in (d) are Pd nano particles

Figure S1. (a) scheme of the sintering set-up; (b) a stacking system in practice.

Figure S2. Schematics of the ECN jig. (a) shows the assembly of the ceramic components for holding the fuel cells; (b) is the bottom view to show the channel of scanning gas distributor. The current collectors on the fuel or air distributor are neglected.

Figure S3. Images of the tri-layer scaffold with (left) and without (right) the frame.

Figure S4. XRD patterns for the $LSV_{ox}$/YSZ (black line) and $LSV_{red}$/electrode (red line).

Figure S5. XRD pattern of LSV/YSZ composite electrode after reduction at 800 $^{o}$C 4.2% steam containing $H_2$. The dots are observed data and the green line is calculated data. The vertical bars are calculated reflections for phases. Upper red represents LSV orthorhombic with symmetry Pbma and bottom black belongs to YSZ cubic with symmetry Fm-3m.